Communication

Wide-Field-of-View Trans-Reflective RGB-Achromatic Metalens for Augmented Reality

Lingcong Luo, Zhengyang Wang, Juntao Li and Haowen Liang *

State Key Laboratory of Optoelectronic Materials and Technologies, School of Physics, Sun Yat-Sen University, Guangzhou 510275, China; luolc@mail2.sysu.edu.cn (L.L.); wangzhy95@mail2.sysu.edu.cn (Z.W.); lijt3@mail.sysu.edu.cn (J.L.)

* Correspondence: lianghw26@mail.sysu.edu.cn

Abstract: In recent years, various solutions for augmented reality (AR) head-mounted displays have been proposed. In order to achieve the dual functions of reflective focusing on virtual images and transparency to the real world, the optical design of AR eyepieces is particularly critical. Designs based on traditional optics still face the problems of huge volume and a limited field of view. Due to their extraordinary phase control ability, portability, easy integration, and other advantages, metalenses have triggered extensive research and found many applications, including providing an innovative solution for AR eyepieces. In this work, we propose a single-layer trans-reflective RGB-achromatic metalens with a large field of view of 90°. The metalens reflects the oblique incident virtual image while maintaining balanced transparency of real-world light. Through simulation, the ability of the metalens to focus light at the wavelengths of 488 nm, 532 nm, and 633 nm with the same focal length and balanced efficiency is validated. Moreover, the metalens is polarization-insensitive to the incident light, thus allowing the elimination of the polarization modulation components, which greatly simplifies the optical structure. Our work demonstrates the great potential of metalenses for AR eyepiece applications.

Keywords: trans-reflective metalens; RGB-achromatic; AR eyepiece

1. Introduction

Metasurfaces are ultrathin two-dimensional devices composed of subwavelength nanostructures [1–3]. By rationally designing the geometric parameters and arrangement of the nanostructures [4], the amplitude, phase, and polarization [5–7] of the incident light can be manipulated so as to realize the anomalous refraction [8], focusing [9], polarization conversion [10], and other functional modulation of beams at a compact distance. Compared with traditional optical lenses, metalenses can achieve more accurate and efficient lensing [11] for both transmitted and reflected wavefronts [12]. Therefore, the complicated phase profiles that are difficult to achieve using traditional lenses can be easily realized by using metalenses. Since metalenses have the advantages of a light weight, easy integration, compatibility with mature semiconductor processes, etc. [13], they have bright prospects for application in portable electronic devices, super-resolution microscopes, future high-performance wearable optical devices, and other applications [14].

Augmented reality (AR) is an emerging display technology that fuses computational virtual information and reality [15]. One of the most important components in AR is the optical combiner. It needs to be transparent to real-world information while being able to project virtual images to the human eyes, allowing the users to naturally experience the fusion of virtual information and reality. Based on this goal, various eyepieces have been proposed, such as free-form optics [16,17], diffractive optical elements (DOEs) [18,19], surface relief gratings (SRGs) [20,21], and holographic optics (HOEs) [22,23]. However, these solutions usually suffer from chromatic aberrations, a limited field of view (FOV),

and low efficiency. In order to reduce the heterogeneity between the virtual scene and the real world, a more compact AR scheme with a wider FOV is urgently needed. Metalenses, with their compact structure and effective phase modulation function, have become one of the most ideal candidates for overcoming such problems [24].

Recently, Shi et al. [25] demonstrated a metasurface AR waveguide to enable on-chip dual-channel semi-transparent holograms. However, this cannot be imaged dynamically due to the static holographic design. In 2018, Lee et al. [26] developed a metalens to realize an ultra-wide FOV and full-color imaging with a large eyebox. However, the prototype includes three dichroic mirrors, thus increasing the complexity and weight of the system. In 2021, a metalens combining Fresnel-diffraction-based 3D computer-generated holography for a near-eye display was proposed by Wang et al. [27]; in the same year, Li et al. [28] demonstrated a virtual reality (VR) scheme based on the RGB-achromatic transmissive metalens. However, the field of views (FOVs) of these metalenses are 31° and less than 10°, respectively. In 2022, Li et al. [29] realized a large-scale meta-optics using an inverse design, and demonstrated its virtual reality (VR) performance. Nevertheless, when it is used in a see-through AR system, such a transmissive metalens also requires an additional optical combiner to merge the virtual images with the real scenes. Li et al. [30] proposed a metalens that could simultaneously function as an off-axis eyepiece and an optical combiner in an AR display, which reduced the complexity of the near-eye AR system; however, the experimental FOV was still narrow. Therefore, a better solution is needed for AR displays to further their applications.

Here, we propose a single-layer see-through trans-reflective achromatic metalens with a wide FOV of 90°, which can be used as an AR display eyepiece. By optimizing a series of center-symmetrical subwavelength meta-units, we demonstrate a three-wavelength achromatic metalens that can reflect and focus oblique incidence light. Furthermore, it maintains transparency under normal incident ambient light, realizing the AR fusion of virtual images and real scenarios. In addition, the metalens is polarization-insensitive to incident light, which requires no extra polarization elements and further simplifies the optical configuration. The final achromatic AR display can be realized only through a single metalens. By using the Maxwellian view, the severe vergence–accommodation conflict (VAC) issue that causes visual fatigue in traditional AR displays can be eliminated, and the final achievable FOV is positively correlated with the numerical aperture (NA) of the designed metalens. This metalens is designed to take into account the key display features, including FOV, chromaticity, and polarization, and its highly integrated performance demonstrates the excellent performance of metasurfaces for AR displays.

2. Design Principle

Figure 1 presents the schematic of the metalens-based AR eyepiece. It reflects the display light and naturally lets the ambient light pass through from the real world simultaneously. The parallel light emitted from the micro-projector is obliquely incident at a design angle of 45° and focused by the metalens, converging to the pupil of the human eye for imaging at the retina. In terms of the virtual image, the Maxwellian view [31] is applied to eliminate the VAC issue caused by long-time eye exposure to conventional 3D devices [32,33]. As shown in the zoomed-in image, when the eye relief is equal to the focal length of the metalens, the virtual light is directly projected on the retina, which is similar to pinhole imaging. In this way, no matter where the eye lens focuses, the virtual image can be clearly imaged at the retina, thereby relieving the VAC fatigue. In this case, the FOV of the AR eyepiece coincides with the corresponding convergence angle of the NA of the lens. Therefore, when the NA increases, the FOV increases accordingly.
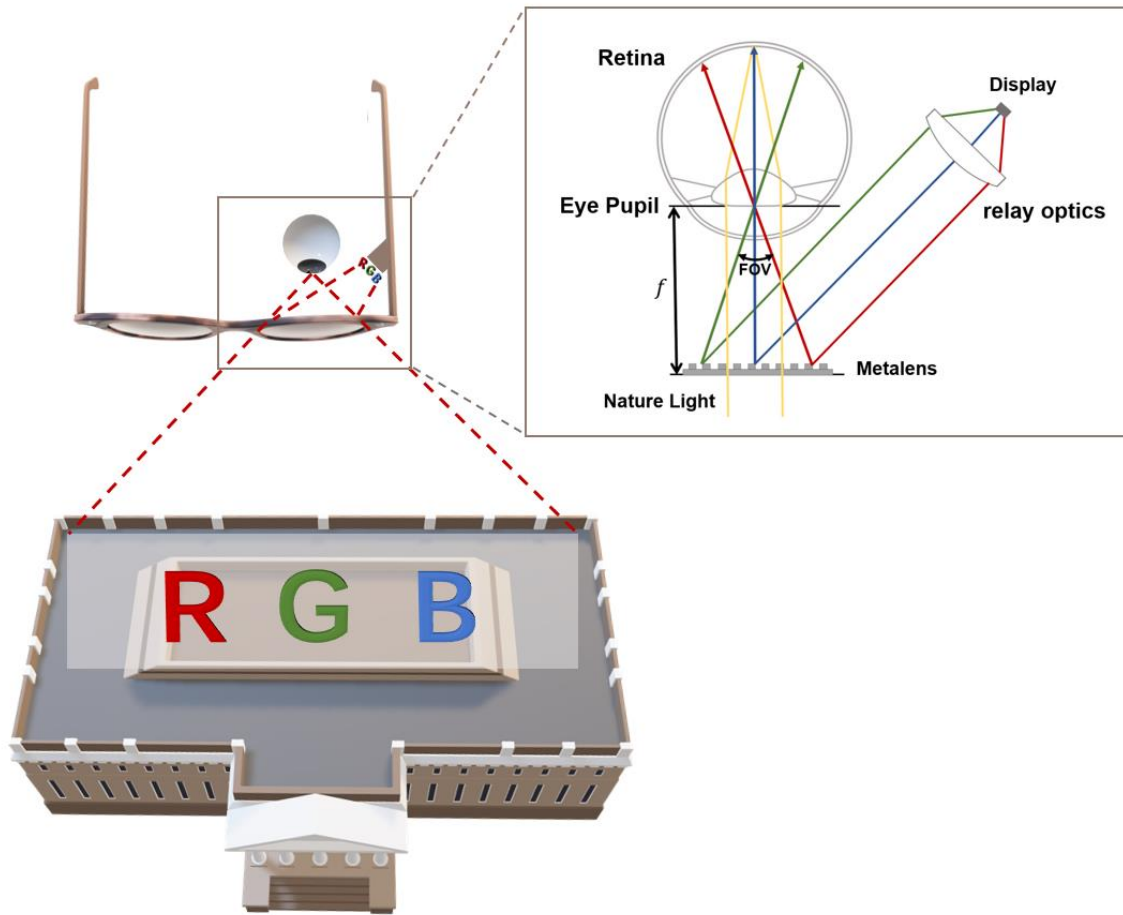
Figure 1. Schematic diagram of the metalens-based near-eye AR display. The micro-projector is mounted on the arm of the glasses and the projected color image is reflected by the metalens to form an enlarged virtual image, while the metalens is also transparent to the real world to provide an immersive augmented reality experience. Zoomed-in image shows the beam path for the Maxwellian view AR display. After passing through the relay optics, the collimated RGB three-wavelength light is reflected and focused to the eye pupil, and then goes directly to the retina without requiring any adjustment of the eyes. The eye relief is equal to the focal length *f*. The FOV is equal to the convergence angle of the metalens.

To achieve reflective focusing for 45° oblique incident light, the metalens should provide a phase shift to convert the incident plane wave into a convergent wave. According to the Fresnel hyperbolic phase equation, the phase profile required for the oblique incident light at the wavelength λ can be written as

$$\varphi(x, y, \lambda_i) = \frac{2\pi}{\lambda_i}\left(\sqrt{x^2 + y^2 + f^2} - f\right) + \varphi_d(\lambda_i), \ \ i = R, G, B \tag{1}$$

where (x,y) are the coordinates of all nanostructures in the lens region, λ_i is the designed wavelength, and *f* is the target focal length, which should be equal to three designed wavelengths. An additional phase $\varphi_d(\lambda_i)$ is introduced to compensate for the off-axis aberrations (the oblique incident angle is θ = 45° to the z axis):

$$\varphi_d(\lambda_i) = -\frac{2\pi}{\lambda_i}y\sin\theta, \ \ i = R, G, B \tag{2}$$

It can be seen from Equations (1) and (2) that the phase profile is a function of wavelength, and the phase profile for each wavelength is no longer center-symmetrical. The phase concentric ring deviates along the incident direction, with a drastic phase change

near the edge of the lens, and the phase required for different wavelengths at each sampling point varies greatly. In order to achieve an identical focal length and balanced efficiency for the three target wavelengths, an achromatic design is required to allow each sampling point on the lens to meet the target phase of the RGB simultaneously [34].

The method for designing multi-wavelength achromatic metalenses can be roughly categorized by single-layer and multi-layer schemes. Since each layer in a multi-layer scheme would increase the absorption of the device, which would result in a severe reduction in the efficiency with regard to focusing both reflective light and transmissive ambient light [35], the single-layer design was chosen in this work. The principle of achromatism achieved using a single-layer metalens involves introducing multiple complex meta-units to increase the lateral degrees of freedom to match the phase for multiple wavelengths [36].

To realize the function of trans-reflection for the AR metalens, crystalline silicon was chosen as the material platform since it has a high refractive index and relatively low absorption for visible wavelengths in the form of meta-units (Supplementary Section S1 shows its complex refractive index) [37–39]. Then, it was necessary to build a structural phase library with high reflectance and a wide range of phase response combinations. Figure 2a shows the 14 kinds of central symmetric building blocks employed in the meta-units to eliminate the polarization dependence. These nanostructures expand the lateral freedom of design and allow obtain a rich combination of multi-wavelength reflection phase responses, which finally leads to an achromatic and polarization-insensitive metalens. Finite-difference time-domain (FDTD) software (Lumerical, Ansys Inc., Canonsburg, PA, USA) was utilized to simulate the nanostructures by scanning the structural parameters of heights (Hs) and periods (Us) to establish a library of corresponding output reflection phases, reflectances, and transmissions at the designed wavelengths of 633 nm, 532 nm, and 488 nm. Then, a group of meta-units with optimal H and U combinations were filtered and optimized from the database by considering the factors of high reflectance, low absorption, and full 2π phase coverage. Among all the factors, high reflectance is the most critical to consider.
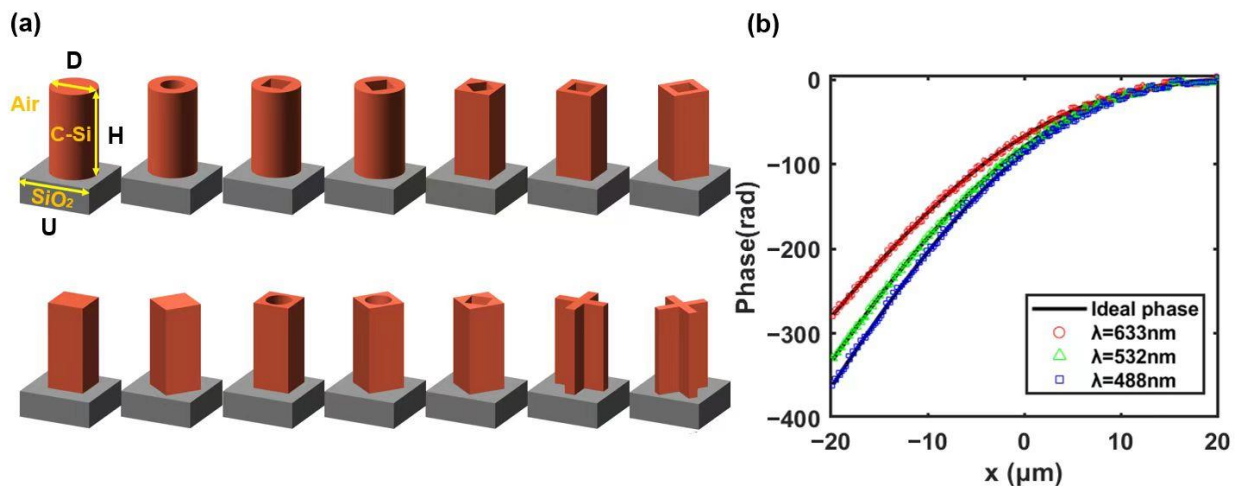

Figure 2. (**a**) The schematics of 14 kinds of center-symmetrical nanostructures, with the silicon nanopillars on the silica substrate. The shapes of the nanopillars include cylinder, rectangle, cross, and so on. Our designed metalens is composed of these meta-units. Abundant multi-wavelength phase responses can be obtained by varying their in-plane geometric parameters; (**b**) a comparison of the ideal phase profile (black lines) and the matched phase of the metalens at the designed wavelengths of 633 nm (red dots), 532 nm (green dots), and 488 nm (blue dots).

In order to improve the phase matching accuracy as much as possible, we compared several phase libraries under different combinations of H and U by searching for the phase and reflectance with the geometrical interval, and we found that H = 175 nm and U = 200 nm were relatively optimal for the built library. With the extensive multi-wavelength phase library, containing 14 kinds of nanostructures, the phase combinations for three wavelengths could be found, and the metalens could finally realize the reflection focusing of three wavelengths of incident light with balanced efficiency. Through the above methods, we designed a metalens with an oblique incidence angle of $\theta = 45°$, an NA = 0.7, and an FOV = 90°. A portion of the intersection of the phase profile is shown in Figure 2b. As can be seen, the actual phase is well matched with the ideal hyperbolic phase profile, which confirms the feasibility of the proposed design.

3. Results

To validate the design, the AR metalens should have been simulated using the FDTD method; however, this method is not ideal for simulating the focusing performance of large-size metalenses. Therefore, the Kirchhoff diffraction integral method [34] was adopted to simulate the focusing performance of a metalens with a diameter of 1 mm and an NA of 0.7. In this method, the light intensity distribution near the focal plane can be simulated by extracting the reflection phase and reflectance provided by the nanostructures at each position of the metalens. To show the polarization insensitivity of the metalens, the reflection and focusing results of the metalens with incident light in linear p and s polarization were simulated, respectively. The cross-sections of the focal spot on the x-z planes of incident light in linear p and s polarization are shown in Figure 3a,b. It can be seen that for both polarizations, the three wavelengths were all focused at the theoretical focal length of $f = 0.5$ mm, which is in good accordance with the expected achromatic focusing performance. Figure 3c also shows the airy spot fitting of the three focal spots for each polarization, revealing that the focusing performance was similar for the two polarizations. The corresponding full width at half-maximums (FWHMs) was 456 nm, 405 nm, and 375 nm for R, G, and B, respectively, which is close to the diffraction limit for NA = 0.7. Additionally, the reflection focusing efficiencies of the three wavelengths were calculated to be 10.71%, 12.2%, and 6.31% for p polarization and 8.73%, 10.55%, and 4.18% for s polarization, respectively. The relatively low focusing efficiency of the 488 nm wavelength was mainly due to the intrinsic absorption of crystalline silicon in short wavelengths. The focusing performance at other wavelengths and the analysis of large-angle deflection for large FOVs are shown in Supplementary Sections S2 and S3, respectively.

In order to investigate the transmission of the metalens to the normal incident ambient light, we used a broadband light source to illuminate the metalens in the FDTD simulation. The corresponding transmission and absorption are shown in Figure 4a,b. The spectrum of the ambient light ranged from 400 nm to 700 nm, and the average transmission of the metalens was 29.8%. Although the absorption of the silicon material led to low transmission at short wavelengths, the overall transmission was roughly uniform. Moreover, through the distribution of the outgoing phase plane in Figure 4c, we verified that the wavefronts were flat in the far field, showing that the real-world image will not be distorted after passing through the metalens. The same conclusion was validated for the case of obliquely incident ambient light (detailed results are shown in Supplementary Table S4).
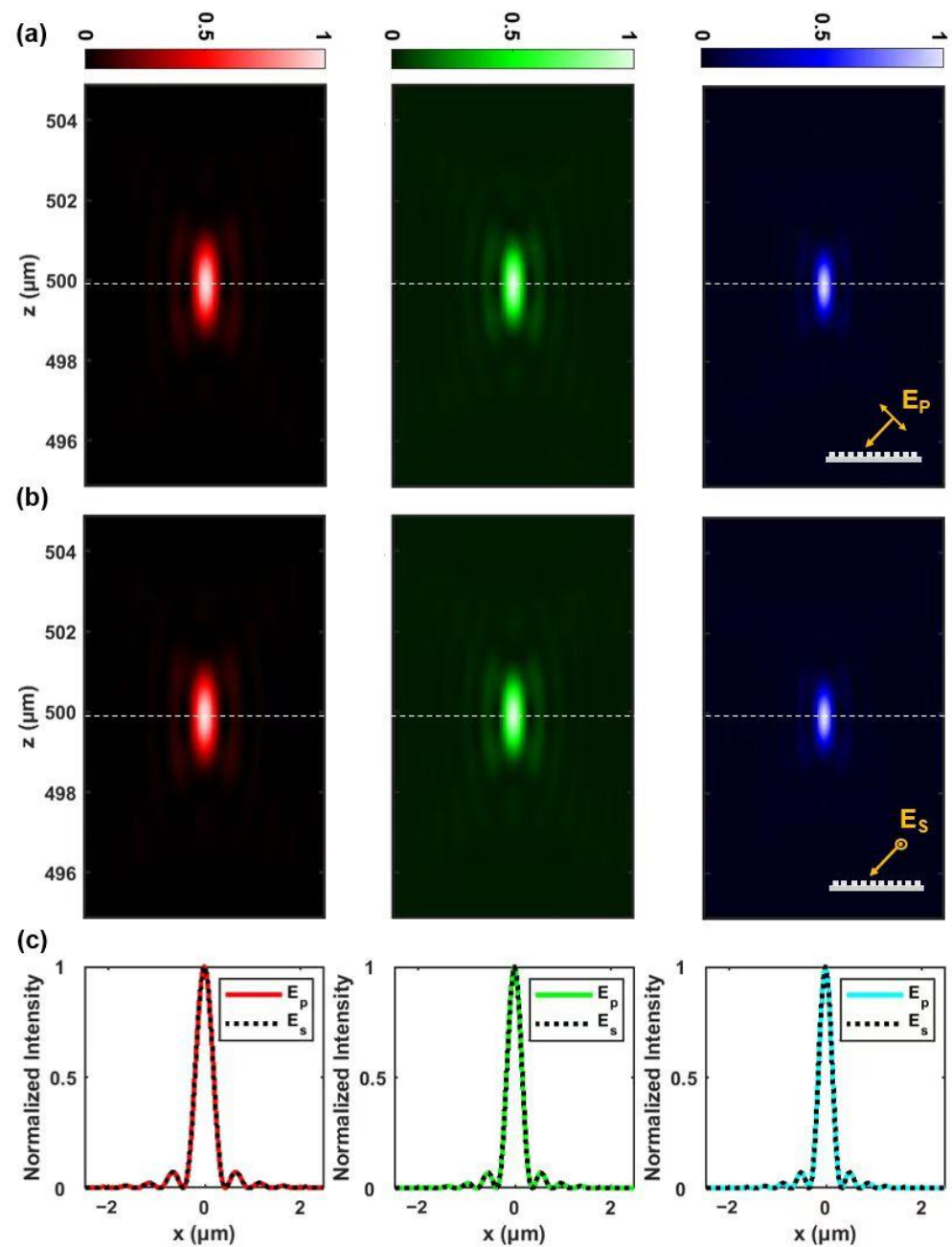
Figure 3. Simulation results of a designed RGB-achromatic metalens (diameter of 1 mm, NA of 0.7, target focal length of 0.5 mm) using the Kirchhoff diffraction integral method: (**a**) normalized intensity distribution in the x-z plane while incident light is in linear p polarization; (**b**) normalized intensity distribution in the x-z plane while incident light is in linear s polarization. The white dot line marks the position of the designed focal length (z = 0.5 mm); (**c**) corresponding normalized intensity profile at the focal plane for the incident light in linear p polarization (solid curve) and in linear s polarization (black dot line).
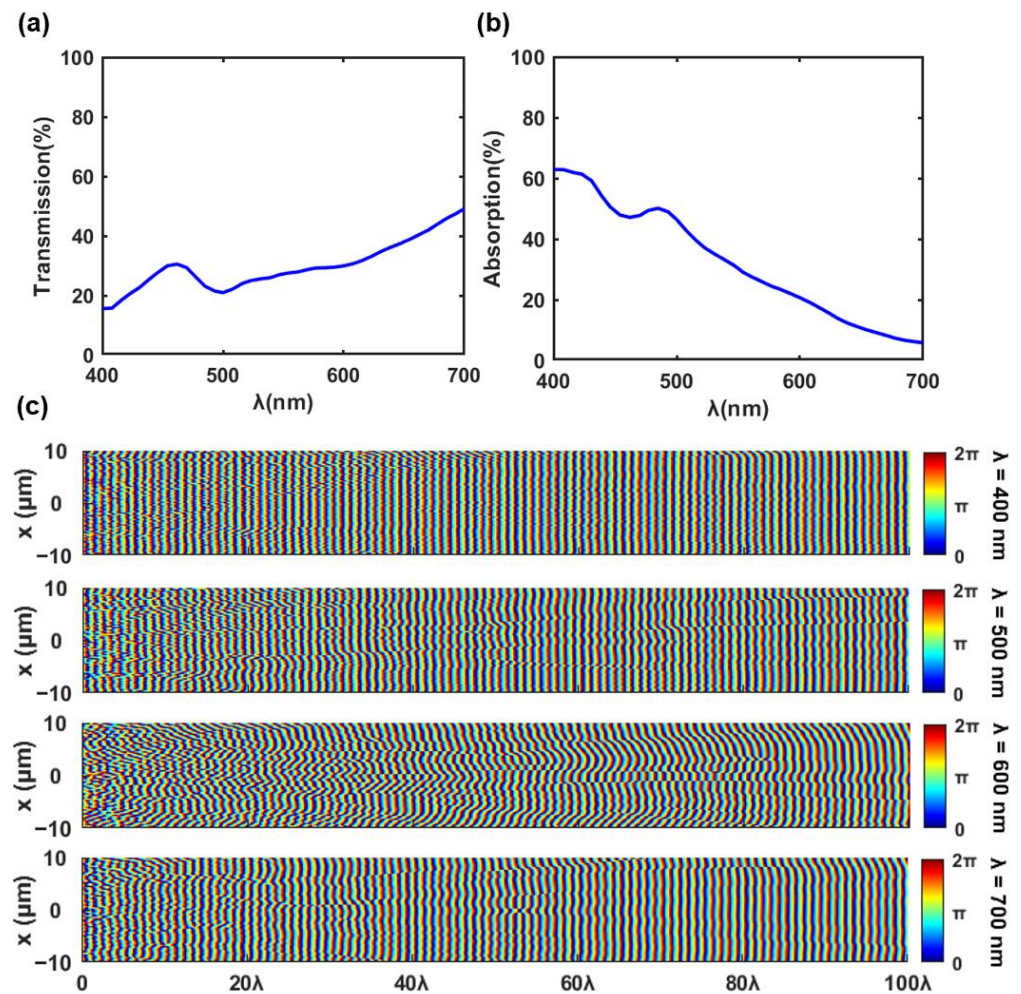
Figure 4. Simulation: (**a**) transmission and (**b**) absorption of the designed metalens to normal incident light ranging from 400 nm to 700 nm; (**c**) distributions of the outgoing phase plane at several wavelengths of ambient light. The wavefronts were flat in the far field, showing that the metalens does not distort the wavefronts of ambient light.

4. Discussion

We determined the reflectance of the three wavelengths tested when selecting nanostructures from the library, ensuring that the reflection focusing efficiency was as high as possible. However, due to the intrinsic absorption of short-wavelength light in silicon, the focusing efficiency is still low. Reducing the absorption and increasing the reflectance are crucial to improve the focusing performance. One possible way to solve this would be to design nonlocal metasurfaces [40] that shape the wavefront only on resonance, which could modify the optical wavefront distinctively at RGB wavelengths and yet stay transparent over the rest of the spectrum. Another approach would be to use reflective distributed Bragg reflectors (DBRs) [41] to increase the reflectance at specific wavelengths.

In the process of optimizing the focusing efficiency of the three wavelengths, we simulated and compared a variety of possible material schemes, but it turns out that these results are worse than the currently obtained values (detailed results are shown in Supplementary Table S5). Since this metalens-based AR eyepiece does not require the assistance of other optical components, such as polarizers and optical combiners, there is no other loss from other optical components and the output focusing efficiency is acceptable compared with the traditional refractive optics and waveguide schemes.

In addition to the Maxwellian view, the multifocal scheme represents another effective approach to mitigating the VAC issue in AR displays with a large eyebox [42]. Reconfig-

urable metalenses, which can tune their focal distance by changing their material states [43] or stretching their substrates [44], play an essential role in enhancing the user experience for metalens-based AR displays.

By utilizing advanced fabrication techniques such as nanoimprinting [26,45,46] and stepper lithography [47], large-size metalens can be fabricated, enabling a practical configuration for AR displays.

To further balance the color efficiency, the initial brightness of the three-wavelength light can be adjusted to ensure that the imaging optical power is consistent. Due to its advantages of high brightness, high efficiency, and the high contrast of displays based on micro-light-emitting diodes [17,48–50], the proposed metalens is expected to become widely used for these AR displays.

5. Conclusions

We propose a trans-reflection achromatic metalens that can be used as an AR eyepiece, which can achieve the fusion of virtual images and real scenarios in a single device. The metalens is transparent under normal incident light over the visible spectrum, ranging from 400 nm to 700 nm, while it has a good reflective focusing performance for RGB light. By adopting a Maxwellian view display, the designed metalens with an NA of 0.7 can achieve a large FOV of 90°. A library of center-symmetrical crystalline silicon-based nanostructures was built to construct the designed metalens. A metalens with an NA of 0.7 and the diameter of 1 mm was simulated, showing the good performance of achromatic focusing and the polarization-insensitive response of the metalens. We foresee this design as having great potential for the next-generation AR near-eye displays.

Supplementary Materials: The following supporting information can be downloaded at: https://www.mdpi.com/article/10.3390/photonics10050590/s1, Section S1: Refractive index of crystalline silicon; Section S2: Focusing performance at other wavelengths; Section S3: Analysis on large-angle deflection for large FOV; Section S4: Transmission for obliquely incident ambient light; Section S5: Other material combinations.

Author Contributions: H.L. and J.L. conceived the idea for the paper. L.L. and Z.W. performed the simulations. L.L., H.L. and J.L. wrote the manuscript. All authors have read and agreed to the published version of the manuscript.

Institutional Review Board Statement: Not applicable.

Informed Consent Statement: Not applicable.

Data Availability Statement: Data is contained within the article or Supplementary Materials.

Conflicts of Interest: The authors declare no conflict of interest regarding this article.

References

1. Wang, D.; Liu, Z.; Wang, H.; Li, M.; Guo, L.J.; Zhang, C. Structural color generation: From layered thin films to optical metasurfaces. *Nanophotonics* **2023**, *12*, 1019–1081. [CrossRef]
2. Luo, X.; Zhang, F.; Pu, M.; Guo, Y.; Li, X.; Ma, X. Recent advances of wide-angle metalenses: Principle, design, and applications. *Nanophotonics* **2021**, *11*, 1–20. [CrossRef]
3. Wei, Q.; Huang, L.; Zentgraf, T.; Wang, Y. Optical wavefront shaping based on functional metasurfaces. *Nanophotonics* **2020**, *9*, 987–1002. [CrossRef]
4. Maguid, E.; Yulevich, I.; Yannai, M.; Kleiner, V.; Brongersma, M.L.; Hasman, E. Multifunctional interleaved geometric-phase dielectric metasurfaces. *Light Sci. Appl.* **2017**, *6*, e17027. [CrossRef]
5. Overvig, A.C.; Shrestha, S.; Malek, S.C.; Lu, M.; Stein, A.; Zheng, C.; Yu, N. Dielectric metasurfaces for complete and independent control of the optical amplitude and phase. *Light Sci. Appl.* **2019**, *8*, 92. [CrossRef]
6. Wu, T.; Zhang, X.; Xu, Q.; Plum, E.; Chen, K.; Xu, Y.; Lu, Y.; Zhang, H.; Zhang, Z.; Chen, X.; et al. Dielectric metasurfaces for complete control of phase, amplitude, and polarization. *Adv. Opt. Mater.* **2022**, *10*, 2101223. [CrossRef]

7. Arbabi, A.; Horie, Y.; Bagheri, M.; Faraon, A. Dielectric metasurfaces for complete control of phase and polarization with subwavelength spatial resolution and high transmission. *Nat. Nanotechnol.* **2015**, *10*, 937–943. [CrossRef]

8. Liu, Y.; Qu, G.; Jiang, X.; Han, J.; Ji, Z.; Liu, Z.; Song, Q.; Yu, S.; Xiao, S. Slanted TiO_2 metagratings for large-angle, high-efficiency anomalous refraction in the visible. *Laser Photonics Rev.* **2023**, 2200712. [CrossRef]

9. Liang, H.; Martins, A.; Borges, B.-H.V.; Zhou, J.; Martins, E.; Li, J.; Krauss, T.F. High performance metalenses: Numerical aperture, aberrations, chromaticity, and trade-offs. *Optica* **2019**, *6*, 1461–1470. [CrossRef]

10. Chen, X.; Zhou, Y.; Ma, X.; Fang, W.; Zhang, W.; Gao, W. Polarization conversion in anisotropic dielectric metasurfaces originating from bound states in the continuum. *Opt. Lett.* **2021**, *46*, 4120–4123. [CrossRef]

11. Khorasaninejad, M.; Chen, W.T.; Devlin, R.C.; Oh, J.; Zhu, A.Y.; Capasso, F. Metalenses at visible wavelengths: Diffraction-limited focusing and subwavelength resolution imaging. *Science* **2016**, *352*, 1190–1194. [CrossRef]

12. Wang, S.; Wu, P.C.; Su, V.C.; Lai, Y.C.; Chu, C.H.; Chen, J.W.; Lu, S.H.; Chen, J.; Xu, B.; Kuan, C.H.; et al. Broadband achromatic optical metasurface devices. *Nat. Commun.* **2017**, *8*, 187. [CrossRef]

13. Khorasaninejad, M.; Capasso, F. Metalenses: Versatile multifunctional photonic components. *Science* **2017**, *358*, eaam8100. [CrossRef]

14. Fu, X.; Liang, H.; Li, J. Metalenses: From design principles to functional applications. *Front. Optoelectron.* **2021**, *14*, 170–186. [CrossRef]

15. Xiong, J.; Hsiang, E.L.; He, Z.; Zhan, T.; Wu, S.T. Augmented reality and virtual reality displays: Emerging technologies and future perspectives. *Light Sci. Appl.* **2021**, *10*, 216. [CrossRef]

16. Hu, X.; Hua, H. High-resolution optical see-through multi-focal-plane headmounted display using freeform optics. *Opt. Express* **2014**, *22*, 13896–13903. [CrossRef]

17. Wei, L.; Li, Y.; Jing, J.; Feng, L.; Zhou, J. Design and fabrication of a compact off-axis see-through head-mounted display using a freeform surface. *Opt. Express* **2018**, *26*, 8550–8565. [CrossRef]

18. Liu, Z.; Pan, C.; Pang, Y.; Huang, Z. A full-color near-eye augmented reality display using a tilted waveguide and diffraction gratings. *Opt. Commun.* **2019**, *431*, 45–50. [CrossRef]

19. Mi, L.; Chen, C.P.; Lu, Y.; Zhang, W.; Chen, J.; Maitlo, N. Design of ensless retinal scanning display with diffractive optical element. *Opt. Express* **2019**, *27*, 20493–20507. [CrossRef]

20. Levola, T.; Laakkonen, P. Replicated slanted gratings with a high refractive index material for in and outcoupling of light. *Opt. Express* **2007**, *15*, 2067–2074. [CrossRef]

21. Bai, B.; Laukkanen, J.; Kuittinen, M.; Siitonen, S. Optimization of nonbinary slanted surface-relief gratings as high-efficiency broadband couplers for light guides. *Appl. Opt.* **2010**, *49*, 5454–5464. [CrossRef] [PubMed]

22. Maimone, A.; Georgiou, A.; Kollin, J.S. Holographic near-eye displays for virtual and augmented reality. *ACM Trans. Graph.* **2017**, *36*, 1–16. [CrossRef]

23. Xiong, J.; Yin, K.; Li, K.; Wu, S.T. Holographic optical elements for augmented reality: Principles, present status, and future perspectives. *Adv. Photonics Res.* **2021**, *2*, 2000049. [CrossRef]

24. Liu, Z.; Wang, D.; Gao, H.; Li, M.; Zhou, H.; Zhang, C. Metasurface-enabled augmented reality display: A review. *Adv. Photon.* **2023**, *5*, 034001. [CrossRef]

25. Shi, Y.; Wan, C.; Dai, C.; Wan, S.; Liu, Y.; Zhang, C.; Li, Z. On-chip meta-optics for semi-transparent screen display in sync with ar projection. *Optica* **2022**, *9*, 670–676. [CrossRef]

26. Lee, G.Y.; Hong, J.Y.; Hwang, S.; Moon, S.; Kang, H.; Jeon, S.; Kim, S.; Jeong, J.H.; Lee, B. Metasurface eyepiece for augmented reality. *Nat. Commun.* **2018**, *9*, 4562. [CrossRef]

27. Wang, C.; Yu, Z.; Zhang, Q.; Sun, Y.; Tao, C.; Wu, F.; Zheng, Z. Metalens eyepiece for 3d holographic near-eye display. *Nanomaterials* **2021**, *11*, 1920. [CrossRef]

28. Li, Z.; Lin, P.; Huang, Y.-W.; Park, J.-S.; Chen, W.T.; Shi, Z.; Qiu, C.-W.; Cheng, J.-X.; Capasso, F. Meta-optics achieves rgb-achromatic focusing for virtual reality. *Sci. Adv.* **2021**, *7*, eabe4458. [CrossRef]

29. Li, Z.; Pestourie, R.; Park, J.S.; Huang, Y.W.; Johnson, S.G.; Capasso, F. Inverse design enables large-scale high-performance meta-optics reshaping virtual reality. *Nat. Commun.* **2022**, *13*, 2409. [CrossRef]

30. Li, Y.; Chen, S.; Liang, H.; Ren, X.; Luo, L.; Ling, Y.; Liu, S.; Su, Y.; Wu, S.-T. Ultracompact multifunctional metalens visor for augmented reality displays. *PhotoniX* **2022**, *3*, 29. [CrossRef]

31. Westheimer, G. The maxwellian view. *Vis. Res.* **1966**, *6*, 669–682. [CrossRef]

32. Hua, H. Enabling focus cues in head-mounted displays. *Proc. IEEE* **2017**, *105*, 805–824. [CrossRef]

33. Takaki, Y.; Fujimoto, N. Flexible retinal image formation by holographic maxwellian-view display. *Opt. Express* **2018**, *26*, 22985–22999. [CrossRef]

34. Feng, W.; Zhang, J.; Wu, Q.; Martins, A.; Sun, Q.; Liu, Z.; Long, Y.; Martins, E.R.; Li, J.; Liang, H. Rgb achromatic metalens doublet for digital imaging. *Nano Lett.* **2022**, *22*, 3969–3975. [CrossRef]

35. Avayu, O.; Almeida, E.; Prior, Y.; Ellenbogen, T. Composite functional metasurfaces for multispectral achromatic optics. *Nat. Commun.* **2017**, *8*, 14992. [CrossRef]

36. Li, H.; Xiao, X.; Fang, B.; Gao, S.; Wang, Z.; Chen, C.; Zhao, Y.; Zhu, S.; Li, T. Bandpass-filter-integrated multiwavelength achromatic metalens. *Photonics Res.* **2021**, *9*, 1384–1390. [CrossRef]

37. Sun, Q.; Liang, H.; Zhang, J.; Feng, W.; Martins, E.R.; Krauss, T.F.; Li, J. Highly efficient air-mode silicon metasurfaces for visible light operation embedded in a protective silica layer. *Adv. Opt. Mater.* **2021**, *9*, 2002209. [CrossRef]

38. Liang, H.; Lin, Q.; Xie, X.; Sun, Q.; Wang, Y.; Zhou, L.; Liu, L.; Yu, X.; Zhou, J.; Krauss, T.F.; et al. Ultrahigh numerical aperture metalens at visible wavelengths. *Nano Lett.* **2018**, *18*, 4460–4466. [CrossRef]

39. Zhou, Z.; Li, J.; Su, R.; Yao, B.; Fang, H.; Li, K.; Zhou, L.; Liu, J.; Stellinga, D.; Reardon, C.P.; et al. Efficient silicon metasurfaces for visible light. *ACS Photonics* **2017**, *4*, 544–551. [CrossRef]

40. Malek, S.C.; Overvig, A.C.; Alù, A.; Yu, N. Multifunctional resonant wavefront-shaping meta-optics based on multilayer and multi-perturbation nonlocal metasurfaces. *Light Sci. Appl.* **2022**, *11*, 246. [CrossRef]

41. Bayati, E.; Wolfram, A.; Colburn, S.; Huang, L.; Majumdar, A. Design of achromatic augmented reality visors based on composite metasurfaces. *Appl. Opt.* **2021**, *60*, 844–850. [CrossRef]

42. Zhan, T.; Xiong, J.; Zou, J.; Wu, S.T. Multifocal displays: Review and prospect. *PhotoniX* **2020**, *1*, 10. [CrossRef]

43. Shalaginov, M.Y.; An, S.; Zhang, Y.; Yang, F.; Su, P.; Liberman, V.; Chou, J.B.; Roberts, C.M.; Kang, M.; Rios, C.; et al. Reconfigurable all-dielectric metalens with diffraction-limited performance. *Nat. Commun.* **2021**, *12*, 1225. [CrossRef]

44. Malek, S.C.; Ee, H.S.; Agarwal, R. Strain Multiplexed Metasurface Holograms on a Stretchable Substrate. *Nano Lett.* **2017**, *17*, 3641–3645. [CrossRef] [PubMed]

45. Zhang, C.; Subbaraman, H.; Li, Q.; Pan, Z.; Ok, J.G.; Ling, T.; Chung, C.-J.; Zhang, X.; Lin, X.; Chen, R.T.; et al. Printed photonic elements: Nanoimprinting and beyond. *J. Mater. Chem. C* **2016**, *4*, 5133–5153. [CrossRef]

46. Yoon, G.; Kim, K.; Huh, D.; Lee, H.; Rho, J. Single-step manufacturing of hierarchical dielectric metalens in the visible. *Nat. Commun.* **2020**, *11*, 2268. [CrossRef]

47. Park, J.S.; Zhang, S.; She, A.; Chen, W.T.; Lin, P.; Yousef, K.M.A.; Cheng, J.X.; Capasso, F. All-glass, large metalens at visible wavelength using deep-ultraviolet projection lithography. *Nano Lett.* **2019**, *19*, 8673–8682. [CrossRef]

48. Wu, Y.; Ma, J.; Su, P.; Zhang, L.; Xia, B. Full-color realization of micro-led displays. *Nanomaterials* **2020**, *10*, 2482. [CrossRef]

49. Huang, Y.; Hsiang, E.L.; Deng, M.Y.; Wu, S.T. Mini-led, micro-led and oled displays: Present status and future perspectives. *Light Sci. Appl.* **2020**, *9*, 105. [CrossRef]

50. Anwar, A.R.; Sajjad, M.T.; Johar, M.A.; Hern'andez-Guti'errez, C.A.; Usman, M.; Lepkowski, S. Recent progress in micro-led-based display technologies. *Laser Photonics Rev.* **2022**, *16*, 2100427. [CrossRef]